NOTE

Magnetic Resonance in Medicine 00:00–00 (2016)

Motion-Robust Cardiac B_1^+ Mapping at 3T Using Interleaved Bloch-Siegert Shifts

Sebastian Weingärtner,[1,2,3]* Fabian Zimmer,[3] Gregory J. Metzger,[2] Kâmil Uğurbil,[2] Pierre-Francois Van de Moortele,[2] and Mehmet Akçakaya[1,2]

Purpose: To develop and evaluate a robust motion-insensitive Bloch-Siegert shift based B_1^+ mapping method in the heart.

Methods: Cardiac Bloch-Siegert B_1^+ mapping was performed with interleaved positive and negative off-resonance shifts and diastolic spoiled gradient echo imaging in 12 heartbeats. Numerical simulations were performed to study the impact of respiratory motion. The method was compared with three-dimensional (3D) actual flip angle imaging (AFI) and two-dimensional (2D) saturated double angle method (SDAM) in phantom scans. Cardiac B_1^+ maps of three different views were acquired in six healthy volunteers using Bloch-Siegert and SDAM during breath-hold and free breathing. In vivo maps were evaluated for inter-view consistency using the correlation coefficients of the B_1^+ profiles along the lines of intersection between the views.

Results: For the Bloch-Siegert sequence, numerical simulations indicated high similarity between breath-hold and free breathing scans, and phantom results indicated low deviation from the 3D AFI reference (normalized root mean square error [NRMSE] = 2.0%). Increased deviation was observed with 2D SDAM (NRMSE = 5.0%) due to underestimation caused by imperfect excitation slice profiles. Breath-hold and free breathing Bloch-Siegert in vivo B_1^+ maps were visually comparable with no significant difference in the inter-view consistency ($P > 0.36$). SDAM showed strongly impaired B_1^+ map quality during free breathing. Inter-view consistency was significantly lower than with the Bloch-Siegert method (breath-hold: $P = 0.014$, free breathing: $P < 0.0001$).

Conclusion: The proposed interleaved Bloch-Siegert sequence enables cardiac B_1^+ mapping with improved inter-view consistency and high resilience to respiratory motion. **Magn Reson Med 000:000–000, 2016. © 2016 International Society for Magnetic Resonance in Medicine**

Key words: cardiac imaging; abdominal imaging; B_1^+ mapping; Bloch-Siegert shift; motion robustness

INTRODUCTION

The advent of quantitative tissue characterization of the myocardium, with its promise for prognostic and diagnostic value in a plethora of cardiomyopathies, has spiked great research interest (1,2) and has triggered a large number of clinical studies (3–7). Available tools for MR-based quantitative tissue characterization in the heart include perfusion (8–10); T_1 (11,12), T_2 (13), and T_2^* relaxation mapping techniques (14–16); and a combination thereof (17,18).

However, many of these approaches, including modified Look–Locker inversion recovery (MOLLI), the most widely used method for myocardial T_1 mapping technique (19), have been reported to be susceptible to the distribution of the radiofrequency (RF) transmit field (B_1^+) and the resulting excitation flip angle (20–23). This problem is particularly severe when moving to high and ultrahigh fields due to the increased heterogeneity of B_1^+ (24–26). It has been demonstrated in several targets (27–31), as well as in the heart (22), that MR-based quantification accuracy greatly improves when correction for B_1^+ is included. Therefore, obtaining reliable absolute B_1^+ magnitude maps ($|B_1^+|$) is critical to achieve accurate quantification in the presence of B_1^+ heterogeneity (32–35).

However, quantification of the transmit B_1 fields in the heart remains challenging due to cardiac and respiratory motion and has received limited attention. Recent studies explored cardiac B_1^+ mapping using the saturated double angle method (SDAM) (36,37), where $|B_1^+|$ is derived from the ratio of two images acquired at different flip angles (38). In SDAM, an additional saturation preparation allows shortening of the repetition time (TR), because waiting for full magnetization recovery is no longer required. Schar et al. (37) proposed the use of SDAM for combined B_1^+ and B_0 mapping of multiple slices in a single breath-hold. To enable rapid image acquisition, accelerated spiral imaging was employed at low spatial resolutions. Similarly, cardiac B_1^+ mapping with SDAM was used for variable flip angle T_1 mapping by Clique et al. (22). In this application, k-space data readout was performed using echo planar imaging (EPI) to enable the data acquisition in a single breath-hold.

Breath-holding is most commonly used in these cardiac B_1^+ mapping methods for respiratory motion compensation. However, the acquisition of two separate images along with the use of segmented k-space readout schemes causes high sensitivity to motion. Hence, B_1^+ map quality may be critically impaired by residual motion, as commonly observed in patients despite breath-holding (39), and remains a major limiting factor for quantitative cardiac imaging.

Among recently proposed B_1^+ mapping techniques, the use of Bloch-Siegert shifts (40) obtained excellent results, enabling the acquisition of B_1^+ maps insensitive to T_1 and B_0 with short TRs. Here, an off-resonant pulse is used to induce a quadratically $|B_1^+|$ dependent phase shift. Bloch-Siegert

[1]Electrical and Computer Engineering, University of Minnesota, Minneapolis, Minnesota, USA.

[2]Center for Magnetic Resonance Research, University of Minnesota, Minneapolis, Minnesota, USA.

[3]Computer Assisted Clinical Medicine, University Medical Center Mannheim, Heidelberg University, Mannheim, Germany.

Grant sponsor: NIH; Grant numbers: R00HL111410, P41EB015894.

*Correspondence to: Sebastian Weingärtner, Ph.D., Electrical and Computer Engineering, University of Minnesota, 200 Union Street SE, Minneapolis, MN 55455. E-mail: sweingae@umn.edu

Received 10 June 2016; revised 15 July 2016; accepted 6 August 2016
DOI 10.1002/mrm.26395
Published online 00 Month 2016 in Wiley Online Library (wileyonlinelibrary.com).

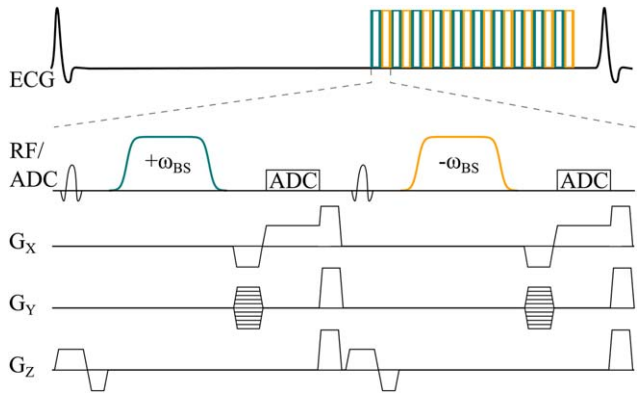

FIG. 1. Sequence diagram depicting the proposed cardiac Bloch-Siegert B_1^+ mapping sequence. A segmented spoiled gradient echo image acquisition is performed with ECG triggering to allow imaging during the diastolic quiescence. Images with negative and positive phase shift, as induced by an off-resonance Fermi pulse, are acquired in an interleaved fashion.

shift based B_1^+ mapping emerged to one of the most widely used methods for transmit field mapping (41–44), including applications to non-proton MRI and spectroscopy (30,31,45). In a recent study, Bloch-Siegert phase shift based $|B_1^+|$ quantification was applied to the heart using a spectroscopic PRESS sequence (46). Although this approach cannot provide spatially resolved maps, as required for image-based parameter quantification, the results indicate improved robustness to respiratory motion.

In this study, we sought to develop a cardiac B_1^+ mapping method based on the Bloch-Siegert phase shift technique combined with an electrocardiogram (ECG)-triggered spoiled gradient echo (SPGR) imaging readout. The positive and negative off-resonance preparations were acquired in an interleaved manner to improve robustness to cardiac and respiratory motion. Numerical simulations and phantom imaging were performed to study sensitivity to motion and to validate quantification accuracy. In vivo experiments were conducted in six healthy subjects to compare the Bloch-Siegert method with the previously proposed SDAM with an EPI readout.

METHODS

Sequence

In the proposed sequence, cardiac B_1^+ maps are acquired by measuring two $|B_1^+|$ dependent Bloch-Siegert shifts as proposed previously (40). The Bloch-Siegert shift is induced using off-resonant Fermi pulses. Imaging is performed with a two-dimensional (2D) SPGR imaging readout. The sequence is performed with ECG triggering to allow imaging in diastolic quiescence. During acquisition, k-space is sampled in a segmented fashion with 10 lines of data acquired for each of the two Bloch-Siegert shifts (Fig. 1). In order to minimize the impact of motion between images obtained with different Bloch-Siegert shifts, positive and negative off-resonance pulses are interleaved for each k-space line acquisition.

An off-resonant Fermi pulse was played between the slice rewinder and the phase-encoding gradient lobes to induce the Bloch-Siegert phase shift: pulse duration $\tau_{BS} = 8.0$ ms, off-resonance shift $\omega_{BS} = \pm 4.0$ kHz, bandwidth containing 99% of the pulse energy = 2.1 kHz. Unless stated otherwise, the total energy of the Fermi pulse was chosen equivalent to that of a rectangular pulse with a nominal flip angle of 60°.

Cardiac Bloch-Siegert B_1^+ mapping was performed with the following imaging parameters: TR = 11.7 ms; echo time (TE) = 9.6 ms; nominal excitation flip angle = 10°; bandwidth = 500 Hz/pixel; field of view (FOV) = $320 \times 320\,mm^2$; in-plane resolution = $2.5 \times 2.5\,mm^2$; slice thickness = 10 mm; and scan time = 12 heartbeats.

Numerical Simulations

Numerical simulations were performed to predict the sensitivity of the proposed cardiac B_1^+ mapping method to respiratory motion. A numerical model of a cardiac short axis slice with compartments for myocardium, blood, epicardial fat, subcutaneous fat, and liver was generated (47) with T_1 relaxation times of 1550, 2500, 380, 380, and 810 ms, respectively (48,49). A static B_1^+ field was modeled with a linearly decreasing trend from foot to head for the purpose of simulation.

Respiration was simulated with sinusoidal diaphragmatic motion along the foot-head dimension. A respiratory frequency of 0.17 Hz was assumed with motion amplitudes between 0 and 3 cm corresponding to four intensities (i.e., breath-hold, shallow breathing, free breathing, heavy breathing) (50). The effect of breathing motion on the B_1^+ map quality was studied using Bloch simulations of the acquisition throughout the respiratory cycle. Dynamic changes in B_1^+ and B_0 throughout the respiratory cycle were neglected.

Imaging

All imaging was performed on a 3T scanner (Magnetom Prisma; Siemens Healthcare, Erlangen, Germany) using the standard body transmit RF coil in dual-drive mode for excitation, with a 30-channel receive array. Standard B_1^+ calibration and shimming were performed, using the default techniques supplied by the vendor (TimTX TrueForm; Siemens Healthcare, Erlangen, Germany).

Phantom

B_1^+ mapping was performed in a cylindrical phantom, containing five spherical compartments with T_1/T_2 times in the range of in vivo muscle tissue (48).

The accuracy and linearity of the proposed technique was compared with the three-dimensional (3D) actual flip angle imaging (AFI) method (51), which was reported to show excellent flip angle accuracy in phantom measurements at 3T (41). This method acquires two interleaved images with different TRs. The following sequence parameters were used: $TR_1/TR_2/TE = 25/125/3.8$ ms; nominal excitation flip angle = 40°–80°; bandwidth = 260 Hz/pixel; FOV = $320 \times 320 \times 160\,mm^3$; in-plane resolution = $2.5 \times 2.5 \times 5\,mm^3$; and scan time = 10 min 20 s.

For further comparison, 2D SDAM, as applied previously for cardiac B_1^+ mapping, was performed with an EPI readout (22). The sequence parameters were: non-refocused EPI imaging train with eight echoes; TE = 1.7 ms; TR = RR interval;

nominal flip angle 1 = 40°–80°; nominal flip angle 2 = 80°–160°; bandwidth = 1500 Hz/pixel; FOV = 320 × 320 mm^2; in-plane resolution = 2.5 × 2.5 mm^2; slice thickness = 10 mm; GRAPPA factor = 2; and sequence duration = 18 heartbeats.

For quantitative comparison the Bloch-Siegert sequence and SDAM were calibrated with respect to the reference 3D AFI method: the transmit power of the Fermi pulse in the Bloch-Siegert sequence and of the slice-selective excitation pulse of the lower flip angle in SDAM were chosen such that the resulting flip angle measurements were identical to 3D AFI at a nominal flip angle of 40°. Subsequently, the transmit power of the Fermi pulse in the Bloch-Siegert sequence and the excitation pulse in SDAM and 3D AFI, were linearly scaled by factors of 1.0, 1.25, . . ., 2.0 corresponding to achieve nominal flip angles of 40°, 50°, . . ., 80°, respectively.

Flip angles were measured from the B_1^+ maps obtained with the three methods using a region of interest (ROI) manually drawn in one of the phantom vials with a T_1 of 1270 ms that is similar to the healthy myocardium at 3T. The accuracy of the flip angle measurements using Bloch-Siegert and SDAM was assessed as the normalized root mean square error (NRMSE) with respect to the 3D AFI method. Furthermore, all three sequences were validated by determining the linearity between the transmit power (nominal flip angle) and the measured flip angle, as proposed by Lutti et al. (52). The linearity was determined using the correlation coefficient.

In Vivo

The imaging protocol was approved by the local institutional review board, and written informed consent was obtained from all participants prior to each examination for this HIPAA-compliant study. B_1^+ mapping was performed in six healthy volunteers (male, n = 2; female, n = 4; age, 33 ± 16 y). Cardiac B_1^+ maps were obtained with the proposed Bloch-Siegert sequence and SDAM in three cardiac orientations: mid-ventricular short axis (SHAX), two chamber (2CH) and four chamber (4CH) views. SAR was recorded for all scans and compared between the two sequences. No in vivo comparison with the 3D AFI reference method was feasible, because there was no sequence variant for cardiac imaging available.

All scans were performed twice to study the impact of respiratory motion: subjects were instructed to hold their breath during the first acquisition, whereas the second acquisition was performed during free breathing.

To quantify consistency between different orientations, the line of intersection within each pair of orientations (e.g., SHAX versus 2CH) was identified independently for each sequence and each acquisition. Subsequently, this line of intersection was restricted to the region of the heart by manually drawing ROIs excluding extracardiac tissue in both views. Consistency was defined as the correlation coefficient between the B_1^+ profiles along the cropped line of intersection in the two views. Statistical significance in the difference between the inter-view consistencies of the different methods at a specific breathing mode (breath-hold/free breathing) across all orientation pairs was assessed using a mixed linear model analysis. Differences in the inter-view consistency of one method between the breathing modes for each pair of orientations were tested for statistical significance using paired Student *t* tests. For all tests, $P < 0.05$ was considered significant.

RESULTS

Numerical Simulations

Figure 2 shows the B_1^+ maps simulated with the numerical torso model for different breathing amplitudes. In Figure 2a, typical motion-induced ghosting artifacts of increasing severity at larger breathing amplitude are readily visible in the baseline images (top row); however, good homogeneity and depiction of the linear B_1^+ field is observed in the maps (bottom row). Although the B_1^+ profiles across the short axis of the heart from the right to the left lateral end clearly show local deviations in the presence of breathing in Fig. 2b, high correlation was preserved even during heavy breathing (R = 1.000/0.9973/0.9943/0.9928 for breath-hold/shallow/free/heavy breathing).

Phantom

Figure 3a depicts the flip angle (average ± standard-deviation) analyzed for each method at all five flip angles. Flip angles assessed with the Bloch-Siegert sequence yielded an NRMSE of 2.0% (range, −3.3% to 2.1%). SDAM showed a higher NRMSE (5.0%) with underestimation of high flip angles by up to 7.5% due to the well-known effect caused by non-rectangular slice profiles of the slice-selective excitation (37). The linearity analysis showed excellent correlation between nominal and measured flip angle for both 3D AFI and Bloch-Siegert B_1^+ maps, with regression coefficients of 0.9999 and 0.9996, respectively. The linearity of SDAM was slightly compromised by slice profile effects, leading to a regression coefficient of 0.9990.

In Vivo

Representative in vivo B_1^+ maps of the heart acquired with the proposed interleaved Bloch-Siegert sequence and the EPI SDAM are depicted in Fig. 4 for acquisitions during breath-hold and free breathing. For the breath-hold acquisitions, a visual inspection of the magnitude images and of the B_1^+ maps generated using the proposed method revealed a clear and smooth depiction of the B_1^+ pattern without noticeable artifacts. By contrast, the magnitude images acquired with SDAM were clearly contaminated with ghosting artifacts attributed to the segmented EPI acquisition. These ghosting artifacts persisted in the calculated B_1^+ maps, although the effect was reduced due to similar artifactual patterns in both baseline images.

For the free breathing acquisitions, noticeable ghosting artifacts could be seen in the phase-encode direction of the magnitude images acquired using the Bloch-Siegert sequence, especially at the level of the anterior chest wall. However, the area of the B_1^+ map covering the cardiac region was well preserved, reproducing closely the pattern measured in the heart under breath-hold conditions. By contrast, the free breathing SDAM acquisition resulted not only in ghosting artifacts distributed over the entire field of view of the baseline images, but also

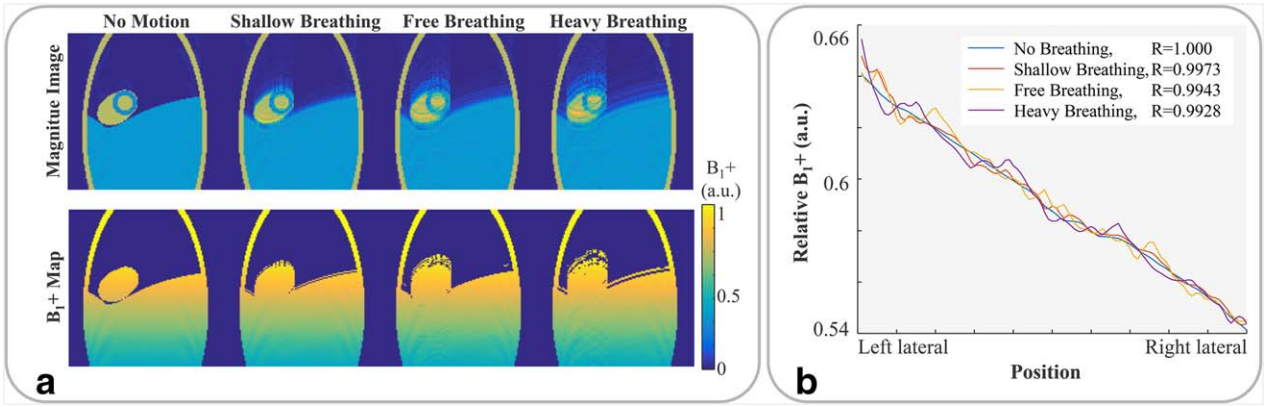

FIG. 2. Numerical simulations studying the sensitivity of the proposed cardiac Bloch-Siegert sequence to respiratory motion. Respiratory-induced translational motion was simulated at four intensities (no motion, shallow breathing, free breathing, and heavy breathing). (**a**) Effect on the simulated magnitude images and quantitative B_1^+ maps. Strong ghosting artifacts are readily visible in the magnitude images, however a clear depiction of the B_1^+ trend is maintained in the B_1^+ maps. (**b**) B_1^+ profile across the heart at various breathing modes. High correlation of the B_1+ profile was obtained even at heavy breathing.

in deeply altered B_1^+ maps, including deterioration in the cardiac regions, rendering these maps unusable.

Average in vivo scan times were 11.1 ± 1.9 s for the Bloch-Siegert sequence and 17.3 ± 3.2 s for SDAM. The SAR burden was significantly higher with the proposed method (0.49 ± 0.11 W/kg) compared with SDAM (0.043 ± 0.007 W/kg).

Figure 5a depicts representative B_1^+ maps acquired with Bloch-Siegert and SDAM in all three orientations during breath-holding. Exemplary lines of intersection as used for the inter-view consistency analysis are indicated. The results of the quantitative inter-view consistency analysis are shown in Fig. 5b. Two major observations can be made regarding the consistency analysis. First, for each of the three inter-view pairs, no significant difference was observed between the inter-view consistency of B_1^+ profiles obtained with the Bloch-Siegert sequence in breath-hold compared with that obtained in free breathing, emphasizing the robustness of the Bloch-Siegert approach against respiration motion ($P > 0.36$). In contrast, SDAM resulted in a markedly reduced consistency between free breathing and breath-hold B_1^+ profiles in SHAX versus 4CH ($P < 0.029$). Second, regardless of the breathing status, the inter-view consistency across all orientation pairs obtained with Bloch-Siegert was always significantly greater than with SDAM. The mixed linear model analysis identified a significant effect of the sequence on the inter-view consistency (difference in consistency [95% confidence interval]): breath-hold: -0.26 [-0.47 to -0.06], $P = 0.014$; free breathing: -0.43 [-0.60 to -0.26], $P < 0.0001$.

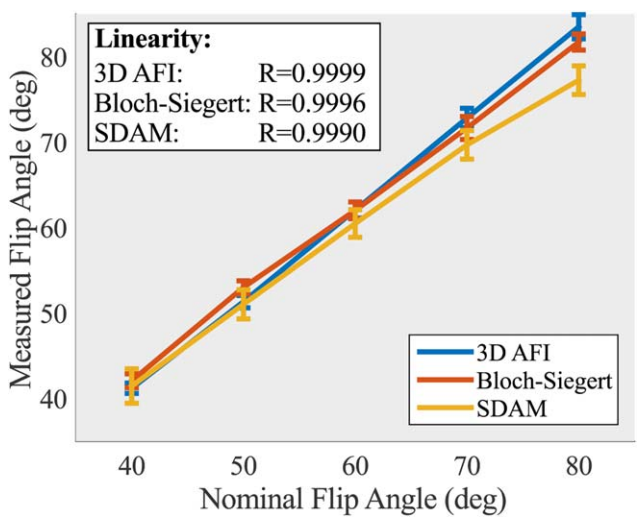

FIG. 3. Phantom evaluation of the proposed Bloch-Siegert sequence and the SDAM EPI method in comparison with a reference 3D AFI method. Flip angle measurements (mean ± standard deviation) within a manually drawn ROI are shown for three B_1^+ mapping methods at multiple nominal flip angles.

DISCUSSION

In this work, we studied a cardiac B_1^+ mapping method based on interleaved Bloch-Siegert shifts induced by a Fermi pulse, followed by SPGR imaging. Despite the use of a segmented acquisition, interleaving the positive and negative off-resonance shifts for each k-space line enabled motion robustness in the cardiac B_1^+ mapping procedure by dramatically reducing the average delay occurring between the two final images. Higher B_1^+ map quality was obtained in comparison with SDAM. This difference was particularly strong during free breathing.

Quantitative mapping of the transmit field in cardiac MRI is challenging due to the presence of cardiac and respiratory motion. To enable the acquisition in a single breath-hold, previous methods employed segmented acquisitions with rapid imaging techniques such as EPI or spiral readouts (36,37). These methods suffer from artifacts in cardiac applications, including susceptibility to motion, hardware inaccuracies, and off-resonance effects (53). This hinders the integration into clinical scan protocols for cardiac applications. The proposed method enables the imaging to be performed with an SPGR Cartesian k-space readout, as commonly used in a multitude of clinical CMR sequences. This confers robustness against acquisition-

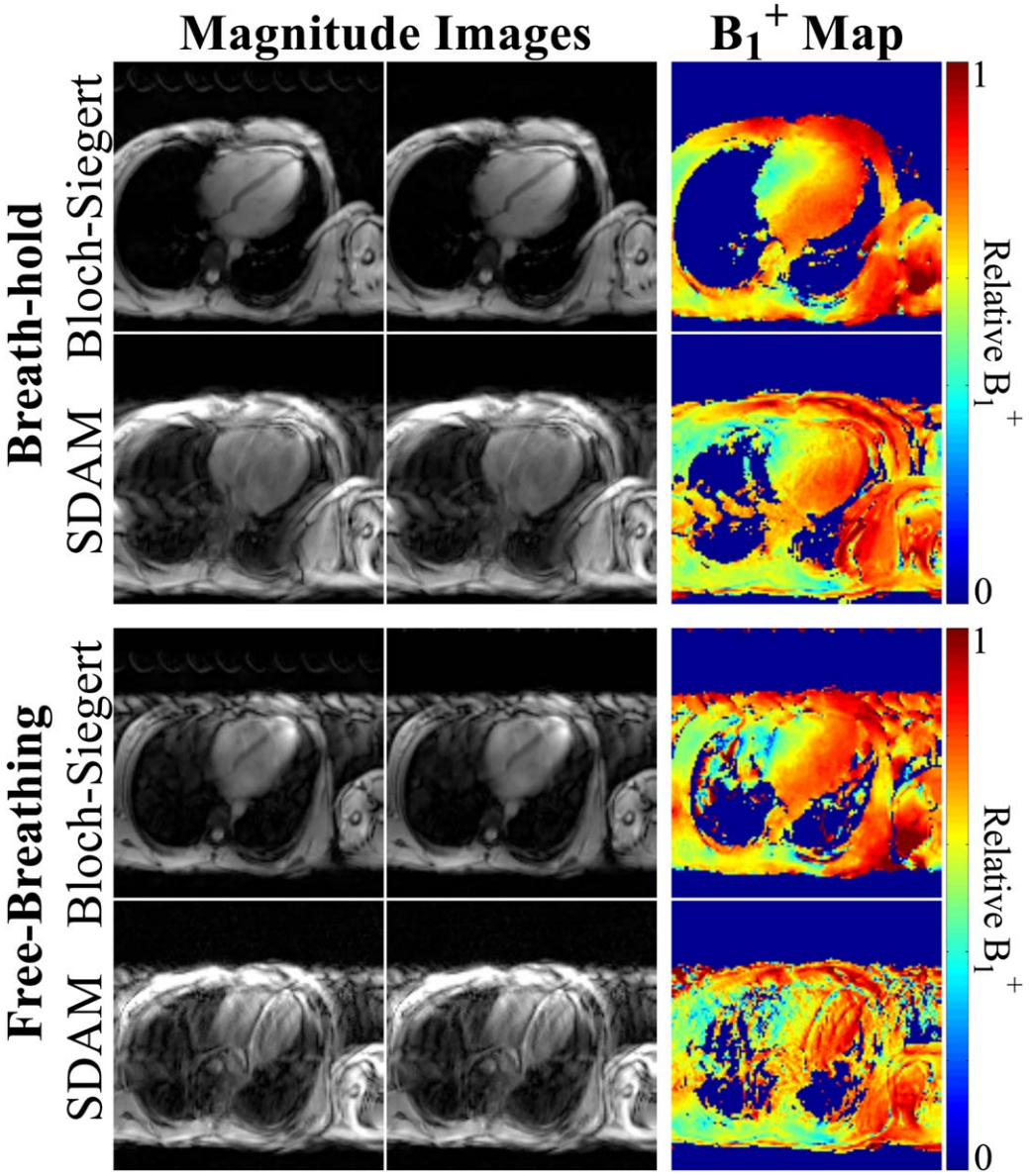

FIG. 4. Representative baseline images and corresponding B_1^+ maps in a cardiac 4CH view acquired using the proposed interleaved Bloch-Siegert method and the SDAM EPI during breath-hold and free breathing. Visually reduced artifact levels, good resilience to respiratory motion, and clear depiction of the B_1^+ trend can be observed in the Bloch-Siegert B_1^+ maps.

specific artifacts while relying on standard reconstruction techniques available on most MRI systems.

The inter-view consistency analysis revealed a systematic trend of decreased consistency in pairs, including the 2CH view when compared with the SHAX versus 4CH pair in all $|B_1^+|$ measurements with both techniques. This is likely because the 2CH views showed flat B_1^+ profiles compared with other views throughout the study. This renders the correlation coefficient used in the consistency analysis more sensitive to small changes in the profile's slope.

Previously published approaches (36,37) employed 2D acquisitions of two separate images with different flip angles. Such approaches are inherently biased by the dependency between the assessed excitation flip angle and the actual slice profile. Although, these inaccuracies can be mitigated by Bloch simulation based corrections, residual error or T_1 dependence might remain (37). Furthermore, double-angle methods are most effective within a range where the higher flip angle is typically larger than 90° (54). This range does not include flip angles commonly used in SPGR cardiac sequences [a typical flip angle is 10°–15° (55)]. The use of the Bloch-Siegert shifts, on the other hand, enables B_1^+ mapping that is independent of the excitation pulse. The B_1^+ encoding Fermi pulses are played separately from the excitation pulse, with a single slice excitation flip angle and profile maintained throughout the entire acquisition.

The proposed method derives B_1^+ maps from GRE images acquired with comparably long echo times; however, this renders the signal sensitive to off-resonance and flow effects, substantially compromising the baseline

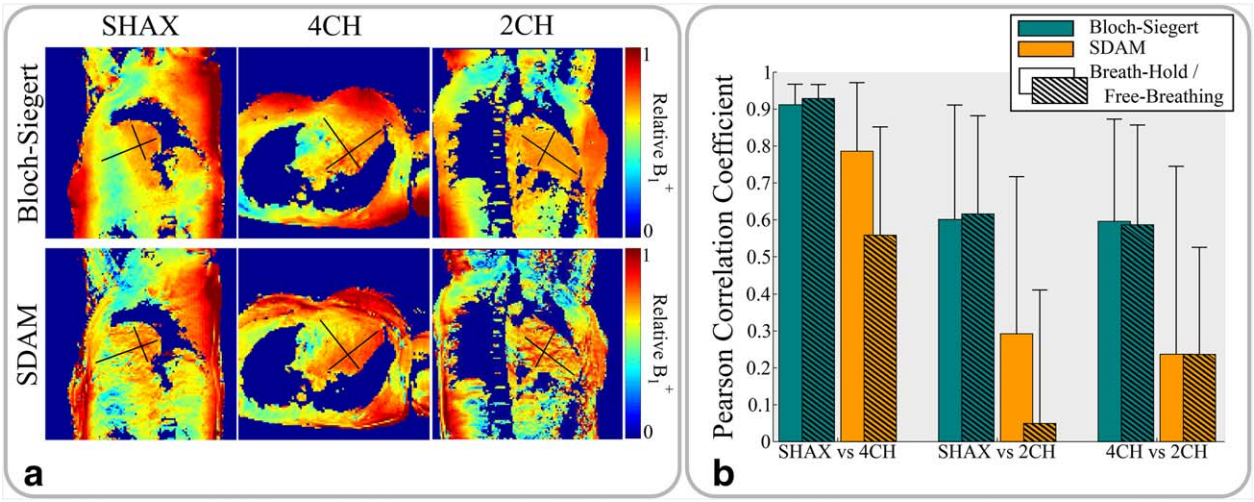

FIG. 5. In vivo inter-view consistency of Bloch-Siegert and SDAM B_1^+ mapping. (**a**) Representative breath-hold B_1^+ maps with black inter-view intersection lines as used in the consistency analysis. (**b**) Inter-view consistency of the B_1^+ profiles along the intersection lines for breath-hold and free breathing scans. Significantly higher inter-view consistency was observed using Bloch-Siegert B_1^+ mapping with similar performance during breath-hold and free breathing.

SNR compared with commonly used cardiac GRE sequences. Short T_2^* times [15–25 ms (56)], especially in the lateral and apical parts, cause rapid signal decay after imaging excitation. Furthermore, "flow void" effects were observed in previous studies with long TE GRE images [TE = 12 ms (57)] in the presence of turbulent jet streams of high velocities. However, flow-induced signal loss can be expected to be minimized by data acquisition during diastole, where flow velocities are an order of magnitude lower than jet stream velocities (58,59). Correspondingly, our data indicate that baseline SNR was sufficient for robust extraction of the phase shift in this healthy cohort. However, chaotic flow patterns (which are commonly observed in patients) or substantially shortened T_2^* (as observed in ultrahigh fields) may potentially cause further reduction in SNR, hindering robust phase extraction. Optimized designs for the off-resonant pulse (60,61) can be employed for these cohorts to substantially shorten the TE and minimize signal loss.

Spatial variations in the flip angle have been reported to hinder the identification of regional variations induced by pathologies in cardiac MRI (62). Furthermore, B_1^+ mapping has been identified as one of the major cofounders in various quantitative imaging applications (21,23,28,63). Robust mapping of the transmit field allows for identification of B_1^+-induced variations and facilitates accurate quantitative measurements (22,29,32,33,35).

Although 1.5T is still the dominant field strength used in cardiac MRI, high-field systems are being used increasingly for cardiac applications. Due to dielectric effects that depend on the Larmor frequency, the transmit field inhomogeneity is increased significantly in high and ultrahigh field applications (24). Cardiac imaging at ultrahigh fields (e.g., 7T) has been facilitated recently by major advances in hardware engineering (25,26,64), including the availability of multichannel transmit systems. With these systems, B_1^+ shimming can be applied to adaptively combine excitation profiles of multitransmit channels/modes for homogenous excitation profiles (65–67). Additionally, tailored RF excitation pulses have been proposed to compensate for transmit field variabilities (68–70). As robust B_1^+ mapping is a prerequisite for these B_1^+ shimming and tailored RF excitation methods, it constitutes a crucial need for overall image quality at ultrahigh fields. Additionally, the B_1^+ field around the heart at 7T has been shown to be dependent on the breathing state, affecting B_1^+ shimming and calibration (71). An extension of the proposed motion-robust cardiac B_1^+ mapping method to ultrahigh field applications potentially allows for robust B_1^+ mapping at various positions in the respiratory cycle. Inaccurate ECG triggering is another challenge of ultrahigh field cardiac imaging. Magneto-hydrodynamic effects lead to frequent misdetections of the R-wave, potentially causing substantial variation in the cardiac phases of ECG-triggered sequences. Although the proposed sequence showed good resilience to respiratory motion, no direct evaluation of the resilience to cardiac motion was performed in this study. The evaluation of cardiac motion sensitivity and the potential benefits of the proposed sequence for inaccurate ECG triggering at 7T will be investigated in future studies.

However, SAR burden has previously been reported to be a major limiting factor for Bloch-Siegert sequences, with particular importance for ultrahigh field imaging (72). Accordingly, the proposed Bloch-Siegert sequence shows significantly higher SAR compared with SDAM. This is primarily due to the high SAR contribution of the off-resonance Fermi pulse (61). Recently, improved encoding pulse designs (60) including adiabatic pulses (61) have been proposed to induce the Bloch-Siegert shift with increased SAR efficiency, enabling B_1^+ mapping at ultrahigh fields. Reduced imaging flip angles and increased scan times might be necessary to reduce the SAR load further. This will be studied in future research to enable the use of the proposed B_1^+ mapping technique for cardiac imaging at 7T.

This study and the proposed methods have several limitations. The numerical simulations represented an

idealized setting, with several simplifications in flow effects, cardiac motion, and dynamic changes in the B_1^+ and B_0 fields throughout the respiratory cycle. Although 3D AFI was used as a reference method in phantom scans, no in vivo comparison of this method could be performed. Due to in-flow effects, cardiac motion, and respiratory motion, a cardiac implementation of this 3D steady-state sequence was beyond the scope of this study. Whereas SDAM enables the acquisition of a slice stack with up to seven parallel slices in a single breath-hold, the proposed Bloch-Siegert method only allows for the acquisition of a single slice. Accelerated data acquisition using, for example, parallel imaging or simultaneous multislice imaging, can be used to facilitate multislice coverage in the proposed breath-hold sequence and will be subject of future studies. Despite the centric view ordering, the use of the long end diastolic imaging window warrants further investigation of the applicability in patients with tachycardia or substantial arrhythmias.

CONCLUSION

In this study, the use of an interleaved Bloch-Siegert SPGR sequence for cardiac B_1^+ mapping was demonstrated in vivo at 3T, with robust B_1^+ map quality in a 12-second breath-hold and high resilience to respiratory motion. Furthermore, a higher consistency between B_1^+ profiles obtained in different views was obtained compared with previously proposed methods. This indicates promise to improve quantitative imaging and RF pulse optimization for various cardiac applications.

REFERENCES

1. Saeed M, Van TA, Krug R, Hetts SW, Wilson MW. Cardiac MR imaging: current status and future direction. Cardiovasc Diagn Ther 2015; 5:290–310.
2. Salerno M, Kramer CM. Advances in parametric mapping with CMR imaging. JACC Cardiovasc Imaging 2013;6:806–822.
3. Cameron D, Siddiqi N, Neil CJ, et al. T1 mapping for assessment of myocardial injury and microvascular obstruction at one week post myocardial infarction. Eur J Radiol 2016;85:279–285.
4. Chen H, Sun J, Kerwin WS, et al. Scan-rescan reproducibility of quantitative assessment of inflammatory carotid atherosclerotic plaque using dynamic contrast-enhanced 3T CMR in a multi-center study. J Cardiovasc Magn Reson 2014;16:51.
5. Taylor AJ, Salerno M, Dharmakumar R, Jerosch-Herold M. T1 mapping: basic techniques and clinical applications. JACC Cardiovasc Imaging 2016;9:67–81.
6. Fontana M, Banypersad SM, Treibel TA, et al. Native T1 mapping in transthyretin amyloidosis. JACC Cardiovasc Imaging 2014;7:157–165.
7. Ferreira VM, Piechnik SK, Robson MD, Neubauer S, Karamitsos TD. Myocardial tissue characterization by magnetic resonance imaging: novel applications of T1 and T2 mapping. J Thorac Imaging 2014;29: 147–154.
8. Bratis K, Mahmoud I, Chiribiri A, Nagel E. Quantitative myocardial perfusion imaging by cardiovascular magnetic resonance and positron emission tomography. J Nucl Cardiol 2013;20:860–870.
9. Heydari B, Kwong RY, Jerosch-Herold M. Technical advances and clinical applications of quantitative myocardial blood flow imaging with cardiac MRI. Prog Cardiovasc Dis 2015;57:615–622.
10. Pelgrim GJ, Handayani A, Dijkstra H, Prakken NH, Slart RH, Oudkerk M, Van Ooijen PM, Vliegenthart R, Sijens PE. Quantitative myocardial perfusion with dynamic contrast-enhanced imaging in MRI and CT: theoretical models and current implementation. Biomed Res Int 2016;2016:1734190.
11. Higgins DM, Moon JC. Review of T1 mapping methods: comparative effectiveness including reproducibility issues. Curr Cardiovasc Imaging Rep 2014;7:1–10.
12. Roujol S, Weingärtner S, Foppa M, Chow K, Kawaji K, Ngo LH, Kellman P, Manning WJ, Thompson RB, Nezafat R. Accuracy, precision, and reproducibility of four T1 mapping sequences: a head-to-head comparison of MOLLI, ShMOLLI, SASHA, and SAPPHIRE. Radiology 2014;272:683–689.
13. Hamlin SA, Henry TS, Little BP, Lerakis S, Stillman AE. Mapping the future of cardiac MR imaging: case-based review of T1 and T2 mapping techniques. Radiographics 2014;34:1594–1611.
14. Kirk P, Roughton M, Porter JB, et al. Cardiac T2* magnetic resonance for prediction of cardiac complications in thalassemia major. Circulation 2009;120:1961–1968.
15. Kondur AK, Li T, Vaitkevicius P, Afonso L. Quantification of myocardial iron overload by cardiovascular magnetic resonance imaging T2* and review of the literature. Clin Cardiol 2009;32:E55–E59.
16. Modell B, Khan M, Darlison M, Westwood MA, Ingram D, Pennell DJ. Improved survival of thalassaemia major in the UK and relation to T2* cardiovascular magnetic resonance. J Cardiovasc Magn Reson 2008;10:42.
17. Akcakaya M, Weingärtner S, Basha TA, Roujol S, Bellm S, Nezafat R. Joint myocardial T1 and T2 mapping using a combination of saturation recovery and T2-preparation. Magn Reson Med 2016;76:888–896.
18. Weingärtner S, Akcakaya M, Roujol S, Basha T, Tschabrunn C, Berg S, Anter E, Nezafat R. Free-breathing combined three-dimensional phase sensitive late gadolinium enhancement and T1 mapping for myocardial tissue characterization. Magn Reson Med 2015;74:1032–1041.
19. Messroghli DR, Radjenovic A, Kozerke S, Higgins DM, Sivananthan MU, Ridgway JP. Modified Look-Locker inversion recovery (MOLLI) for high-resolution T1 mapping of the heart. Magn Reson Med 2004; 52:141–146.
20. Kellman P, Hansen MS. T1-mapping in the heart: accuracy and precision. J Cardiovasc Magn Reson 2014;16:2.
21. Wang P, Xue Y, Zhao X, Yu J, Rosen M, Song HK. Effects of flip angle uncertainty and noise on the accuracy of DCE-MRI metrics: comparison between standard concentration-based and signal difference methods. Magn Reson Imaging 2015;33:166–173.
22. Clique H, Cheng HL, Marie PY, Felblinger J, Beaumont M. 3D myocardial T1 mapping at 3T using variable flip angle method: pilot study. Magn Reson Med 2014;71:823–829.
23. Helms G, Dathe H, Dechent P. Quantitative FLASH MRI at 3T using a rational approximation of the Ernst equation. Magn Reson Med 2008; 59:667–672.
24. Vaughan JT, Garwood M, Collins CM, et al. 7T vs. 4T: RF power, homogeneity, and signal-to-noise comparison in head images. Magn Reson Med 2001;46:24–30.
25. Snyder CJ, DelaBarre L, Metzger GJ, van de Moortele PF, Akgun C, Ugurbil K, Vaughan JT. Initial results of cardiac imaging at 7 Tesla. Magn Reson Med 2009;61:517–524.
26. von Knobelsdorff-Brenkenhoff F, Frauenrath T, Prothmann M, Dieringer MA, Hezel F, Renz W, Kretschel K, Niendorf T, Schulz-Menger J. Cardiac chamber quantification using magnetic resonance imaging at 7 Tesla—a pilot study. Eur Radiol 2010;20:2844–2852.
27. Deoni SC. High-resolution T1 mapping of the brain at 3T with driven equilibrium single pulse observation of T1 with high-speed incorporation of RF field inhomogeneities (DESPOT1-HIFI). J Magn Reson Imaging 2007;26:1106–1111.
28. Sung K, Daniel BL, Hargreaves BA. Transmit B1 + field inhomogeneity and T1 estimation errors in breast DCE-MRI at 3 Tesla. J Magn Reson Imaging 2013;38:454–459.
29. Sung K, Saranathan M, Daniel BL, Hargreaves BA. Simultaneous T(1) and B(1) (+) mapping using reference region variable flip angle imaging. Magn Reson Med 2013;70:954–961.
30. Lommen J, Konstandin S, Kramer P, Schad LR. Enhancing the quantification of tissue sodium content by MRI: time-efficient sodium B1 mapping at clinical field strengths. NMR Biomed 2016;29:129–136.
31. Schulte RF, Sacolick L, Deppe MH, Janich MA, Schwaiger M, Wild JM, Wiesinger F. Transmit gain calibration for nonproton MR using the Bloch-Siegert shift. NMR Biomed 2011;24:1068–1072.
32. Venkatesan R, Lin W, Haacke EM. Accurate determination of spin-density and T1 in the presence of RF-field inhomogeneities and flip-angle miscalibration. Magn Reson Med 1998;40:592–602.
33. Sled JG, Pike GB. Correction for B(1) and B(0) variations in quantitative T(2) measurements using MRI. Magn Reson Med 2000;43:589–593.
34. Wang J, Qiu M, Kim H, Constable RT. T1 measurements incorporating flip angle calibration and correction in vivo. J Magn Reson 2006;182:283–292.

35. Samson RS, Wheeler-Kingshott CA, Symms MR, Tozer DJ, Tofts PS. A simple correction for B1 field errors in magnetization transfer ratio measurements. Magn Reson Imaging 2006;24:255–263.
36. Cunningham CH, Pauly JM, Nayak KS. Saturated double-angle method for rapid B1 + mapping. Magn Reson Med 2006;55:1326–1333.
37. Schar M, Vonken EJ, Stuber M. Simultaneous B(0)- and B(1)+-map acquisition for fast localized shim, frequency, and RF power determination in the heart at 3 T. Magn Reson Med 2010;63:419–426.
38. Insko EK, Bolinger L. Mapping of the radiofrequency field. J Magn Reson A 1993;103:82–85.
39. Roujol S, Foppa M, Weingärtner S, Manning WJ, Nezafat R. Adaptive registration of varying contrast-weighted images for improved tissue characterization (ARCTIC): application to T1 mapping. Magn Reson Med 2015;73:1469–1482.
40. Sacolick LI, Wiesinger F, Hancu I, Vogel MW. B1 mapping by Bloch-Siegert shift. Magn Reson Med 2010;63:1315–1322.
41. Pohmann R, Scheffler K. A theoretical and experimental comparison of different techniques for B(1) mapping at very high fields. NMR Biomed 2013;26:265–275.
42. Carinci F, Santoro D, von Samson-Himmelstjerna F, Lindel TD, Dieringer MA, Niendorf T. Characterization of phase-based methods used for transmission field uniformity mapping: a magnetic resonance study at 3.0 T and 7.0 T. PLoS One 2013;8:e57982.
43. Sharma A, Tadanki S, Jankiewicz M, Grissom WA. Highly-accelerated Bloch-Siegert |B1+| mapping using joint autocalibrated parallel image reconstruction. Magn Reson Med 2014;71:1470–1477.
44. Saranathan M, Khalighi MM, Glover GH, Pandit P, Rutt BK. Efficient Bloch-Siegert B1 (+) mapping using spiral and echo-planar readouts. Magn Reson Med 2013;70:1669–1673.
45. Lau AZ, Chen AP, Cunningham CH. Integrated Bloch-Siegert B(1) mapping and multislice imaging of hyperpolarized (1)(3)C pyruvate and bicarbonate in the heart. Magn Reson Med 2012;67:62–71.
46. Clarke WT, Robson MD, Rodgers CT. Bloch-Siegert B1+-mapping for human cardiac P-MRS at 7 Tesla. Magn Reson Med 2015. doi: 10.1002/mrm.26005.
47. Weingärtner S, Akcakaya M, Basha T, Kissinger KV, Goddu B, Berg S, Manning WJ, Nezafat R. Combined saturation/inversion recovery sequences for improved evaluation of scar and diffuse fibrosis in patients with arrhythmia or heart rate variability. Magn Reson Med 2014;71:1024–1034.
48. Stanisz GJ, Odrobina EE, Pun J, Escaravage M, Graham SJ, Bronskill MJ, Henkelman RM. T1, T2 relaxation and magnetization transfer in tissue at 3T. Magn Reson Med 2005;54:507–512.
49. Meßner N, Weingärtner S, Budjan J, Loßnitzer D, Mattler U, Papavassiliu T, Schad L, Zöllner F. Myocardial T1- and ECV-Mapping at 3 Tesla Using the Saturation-Recovery Techniques SASHA and SAPPHIRE. In Proceedings of the 24th Annual Meeting of ISMRM, Singapore, Singapore, 2016. p. 3152.
50. Wang Y, Riederer SJ, Ehman RL. Respiratory motion of the heart: kinematics and the implications for the spatial resolution in coronary imaging. Magn Reson Med 1995;33:713–719.
51. Yarnykh VL. Actual flip-angle imaging in the pulsed steady state: a method for rapid three-dimensional mapping of the transmitted radiofrequency field. Magn Reson Med 2007;57:192–200.
52. Lutti A, Stadler J, Josephs O, Windischberger C, Speck O, Bernarding J, Hutton C, Weiskopf N. Robust and fast whole brain mapping of the RF transmit field B1 at 7T. PLoS One 2012;7:e32379.
53. Block KT, Frahm J. Spiral imaging: a critical appraisal. J Magn Reson Imaging 2005;21:657–668.
54. Morrell GR, Schabel MC. An analysis of the accuracy of magnetic resonance flip angle measurement methods. Phys Med Biol 2010;55: 6157–6174.
55. Kim RJ, Shah DJ, Judd RM. How we perform delayed enhancement imaging. J Cardiovasc Magn Reson 2003;5:505–514.
56. Zaman A, Higgins DM, Motwani M, Kidambi A, Kouwenhoven M, Kozerke S, Greenwood JP, Plein S. Robust myocardial T2 and T2* mapping at 3T using image-based shimming. J Magn Reson Imaging 2015;41:1013–1020.
57. Didier D, Ratib O, Lerch R, Friedli B. Detection and quantification of valvular heart disease with dynamic cardiac MR imaging. Radiographics 2000;20:1279–1299.
58. Kim WY, Walker PG, Pedersen EM, Poulsen JK, Oyre S, Houlind K, Yoganathan AP. Left ventricular blood flow patterns in normal subjects: a quantitative analysis by three-dimensional magnetic resonance velocity mapping. J Am Coll Cardiol 1995;26:224–238.
59. O'Brien KR, Cowan BR, Jain M, Stewart RA, Kerr AJ, Young AA. MRI phase contrast velocity and flow errors in turbulent stenotic jets. J Magn Reson Imaging 2008;28:210–218.
60. Jankiewicz M, Gore JC, Grissom WA. Improved encoding pulses for Bloch-Siegert B1(+) mapping. J Magn Reson 2013;226:79–87.
61. Khalighi MM, Rutt BK, Kerr AB. Adiabatic RF pulse design for Bloch-Siegert B1 + mapping. Magn Reson Med 2013;70:829–835.
62. Greenman RL, Shirosky JE, Mulkern RV, Rofsky NM. Double inversion black-blood fast spin-echo imaging of the human heart: a comparison between 1.5T and 3.0T. J Magn Reson Imaging 2003;17:648–655.
63. Coolen BF, Geelen T, Paulis LE, Nauerth A, Nicolay K, Strijkers GJ. Three-dimensional T1 mapping of the mouse heart using variable flip angle steady-state MR imaging. NMR Biomed 2011;24:154–162.
64. Suttie JJ, Delabarre L, Pitcher A, et al. 7 Tesla (T) human cardiovascular magnetic resonance imaging using FLASH and SSFP to assess cardiac function: validation against 1.5 T and 3 T. NMR Biomed 2012;25:27–34.
65. Ibrahim TS, Lee R, Baertlein BA, Abduljalil AM, Zhu H, Robitaille PM. Effect of RF coil excitation on field inhomogeneity at ultra high fields: a field optimized TEM resonator. Magn Reson Imaging 2001; 19:1339–1347.
66. Mao W, Smith MB, Collins CM. Exploring the limits of RF shimming for high-field MRI of the human head. Magn Reson Med 2006;56: 918–922.
67. Hoult DI, Phil D. Sensitivity and power deposition in a high-field imaging experiment. J Magn Reson Imaging 2000;12:46–67.
68. Liu H, Matson GB. Radiofrequency pulse designs for three-dimensional MRI providing uniform tipping in inhomogeneous B(1) fields. Magn Reson Med 2011;66:1254–1266.
69. Saekho S, Yip CY, Noll DC, Boada FE, Stenger VA. Fast-kz three-dimensional tailored radiofrequency pulse for reduced B1 inhomogeneity. Magn Reson Med 2006;55:719–724.
70. Sung K, Nayak KS. B1 + compensation in 3T cardiac imaging using short 2DRF pulses. Magn Reson Med 2008;59:441–446.
71. Schmitter S, Wu X, Ugurbil K, Van de Moortele PF. Design of parallel transmission radiofrequency pulses robust against respiration in cardiac MRI at 7 Tesla. Magn Reson Med 2015;74:1291–1305.
72. van der Kolk AG, Hendrikse J, Zwanenburg JJ, Visser F, Luijten PR. Clinical applications of 7 T MRI in the brain. Eur J Radiol 2013;82: 708–718.